ACS APPLIED ENERGY MATERIALS

www.acsaem.org Letter

Fluoride-Free Surface Passivation Enables Low-Concentration Nonflammable Electrolytes for K-Ion Batteries

Andrew W. Ells, Pablo J. Buitrago Botero, Bret Schumacher, Lakshmi Bhai, and Lauren E. Marbella*

Cite This: *ACS Appl. Energy Mater.* 2024, 7, 10245−10250 Read Online

ABSTRACT: Here, we show that a low-concentration (1 M) KPF_6 electrolyte combining ethylene carbonate, propylene carbonate, and triethyl phosphate (TEP) achieves stable cycling with graphite anodes, retains high ionic conductivity, and is nonflammable. Surface characterization of the solid−electrolyte interphase (SEI) reveals that KPF_6 does not reduce to KF. Instead, TEP results in the accumulation of inorganic phosphates that passivate against reductive decomposition of carbonate solvents and lessen resistance to K-ion transport through the SEI. Overall, carbonate/phosphate solvent mixtures serve as a nonflammable baseline for future engineering of the SEI layer that eliminates ionically insulating fluorinated phases.

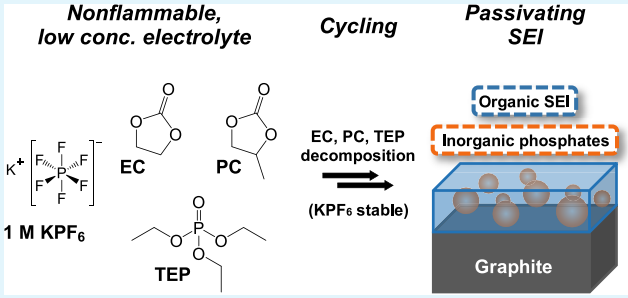

KEYWORDS: *battery, K-ion, beyond Li, solid−electrolyte interphase, electrolyte engineering, nonflammable, nuclear magnetic resonance, fluoride-free*

The transition to a renewable energy ecosystem requires widespread, affordable electrochemical energy storage for grid and transportation applications. Li-ion batteries (LIBs) currently dominate the commercial energy storage market, but supply chain concerns for Li and other critical minerals motivate the development of new battery chemistries.[1,2] Na-ion batteries have subsequently been studied, but longevity and volumetric energy density concerns have slowed rapid adoption.[3] In turn, K-ion batteries (KIBs) offer compelling advantages as a Li alternative. Most importantly, K can reversibly intercalate into graphite (Gr), while Na cannot,[4,5] enabling use of the most popular commercial anode.[1,2]

At present, 2 M KFSI in TEP is one of the preeminent electrolytes for KIBs because it can achieve a Coulombic efficiency (CE) of 99.7% for K||Gr over 300 cycles[6] and suppress electrolyte ignition through a radical trap/gas phase mechanism.[6−8] Higher salt concentrations (>2.5 M) are required in full cells assembled with Prussian blue analogues to achieve high CE and long cycle life,[9] suggesting additional issues with interfacial instability at the cathode. Despite some success with 2 M KFSI in TEP, there are significant drawbacks associated with high-concentration electrolytes (HCEs), including high viscosity, low ionic conductivity, and high salt cost. These properties sacrifice many of the benefits touted for KIBs (e.g., a cheaper alternative to LIBs and fast charging capabilities[1,2]), rendering KIB technologies of little use if this is the electrolyte of choice.

Unfortunately, low-concentration (∼1 M) K electrolytes with TEP as the sole solvent are incompatible with Gr anodes due to the inability to form a passivating SEI and/or cointercalation, making it difficult to retain flame-retardant properties in practical applications.[6] Replacing TEP with conventional carbonate solvent mixtures [e.g., ethylene carbonate (EC) with linear carbonates such as dimethyl carbonate (DMC) or diethyl carbonate (DEC)] prevents exfoliation when paired with ∼1 M KPF_6 or KFSI, but the linear carbonate lowers the vapor flammability of the electrolyte[10] and the carbonate-derived organic solid−electrolyte interphase (SEI) fails to enable reversible K intercalation over extended cycling.[5] For example, 1 M KPF_6 in EC/DMC exhibits CE values of <90% during the first 100 cycles, which then rapidly falls below 80% using a C-rate of C/14.[5] Switching the solvent to EC/PC prevents this rollover failure, which is consistent with findings from the Na-ion battery literature that EC/PC base formulations improve performance and linear carbonates are detrimental to battery health.[11] In this vein, ∼50% capacity fade was observed for Gr electrodes cycled in 0.8 M KPF_6 in EC/DEC after only 50 cycles when cycled at C/2.[12] Efforts to improve the capacity retention with additives that have been successful in LIBs, like fluoroethylene carbonate (FEC), fail in KIBs due to the accumulation of KF and K_2CO_3 on the electrode surface.[13,14] We believe that KF is particularly

Received: October 10, 2024
Revised: November 1, 2024
Accepted: November 6, 2024
Published: November 13, 2024

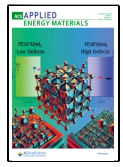

https://doi.org/10.1021/acsaem.4c02579
ACS Appl. Energy Mater. 2024, 7, 10245−10250

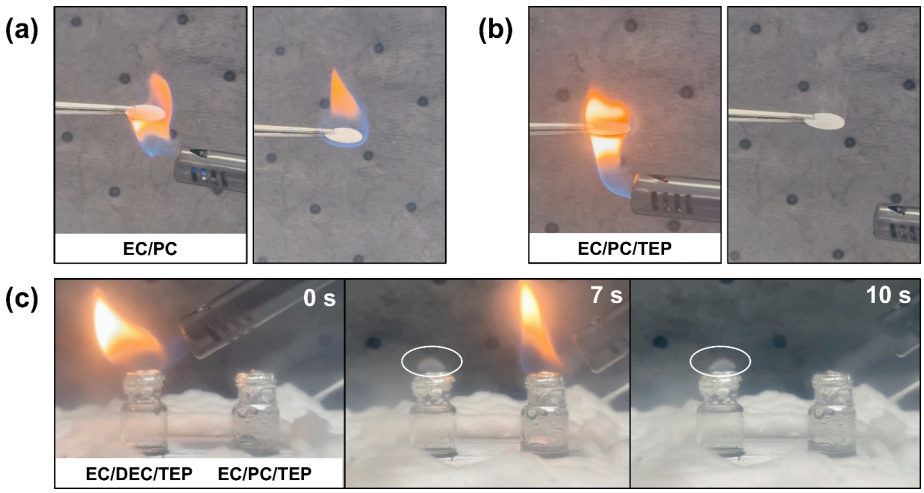

Figure 1. Flame tests of glass fiber separators soaked in (a) EC/PC and (b) EC/PC with 20 vol % TEP. (c) Various time points of a vapor flammability test at 200 °C for EC/DEC with 20 vol % TEP (left) and EC/PC with 20 vol % TEP (right). The white ring highlights a self-sustaining flame from vapor ignition in the electrolyte, which contains DEC.

insidious because it is expected to exhibit significantly lower ionic conductivity values than LiF (already at 10^{-13} S cm^{-1})[15] and higher activation barriers to ion diffusion.[13,16,17]

One property that has been overlooked in the design of low-concentration KIB electrolytes is the exceptional reductive and hydrolytic stability of the PF_6^- anion.[18,19] By avoiding the formation of KF and poorly passivating compounds like K_xPF_y and $K_xPO_yF_z$ during electrochemical cycling, electrolytes formulated with 1 M KPF_6 present a unique opportunity to tune both electrolyte and interphase properties. The key to unlocking the design space for low-concentration K electrolytes is to incorporate solvents that impart desirable properties in the bulk and that will generate inorganic SEI species that can conduct K-ions. Here, we hypothesize that we can attain a nonflammable, low-concentration KIB electrolyte by using TEP as a cosolvent in a nonvolatile carbonate formulation with the intention of simultaneously reducing the solvents and embedding ionically conductive phases, like K_xPO_y (e.g., the ionic conductivity of K_3PO_4 at room temperature = 9×10^{-6} S cm^{-1} with negligible electronic conductivity in the bulk[20]), in the organic interphase.

We begin by screening different percentages of TEP (0, 20, and 50 vol %) in a mixture of EC/propylene carbonate (PC) in hard carbon K half-cells (K||HC), where PC is preferred over linear carbonates due to its higher boiling point (Table S1). Screening with K||HC allows us to ensure that we deliver the proper amount of TEP and achieve the subsequent decomposition products in the SEI that enable reversible K intercalation at high loading values (>3 mg cm^{-2}) and at appreciable rates (C/5) because transport is less of a concern in HC than Gr. The electrochemical cycling data shown in Figure S1 indicate that electrolytes with 1 M KPF_6 with EC/PC + 20 vol % TEP display higher capacity within the first 10 cycles at C/5 [168 mAh g^{-1} compared to those that contain 0 or 50 vol % TEP (158 and 137 mAh g^{-1}, respectively)]. As expected, when TEP is the sole solvent, cells fail to reversibly cycle and Gr shows evidence of solvent cointercalation (Figure S2).

From here, we assess the safety advantages of utilizing EC/PC with 20 vol % TEP rather than the conventional mix of EC and a linear carbonate such as DEC, even when combined with TEP. Because EC and PC have the lowest volatility of conventional carbonate solvents, they require the lowest concentration of flame retardant to make a nonflammable mixture.[21] In a flame test where glass fiber separators were soaked in electrolyte and ignited (Figure 1a,b), we found that the self-extinguish time (the duration of a self-sustaining flame per unit mass of electrolyte) of 1 M KPF_6 in EC/PC is 109 s g^{-1} and that adding >10 vol % TEP prevents combustion outright. Therefore, a solvent mix of 1 M KPF_6 in EC/PC with 20 vol % TEP was selected for this study (recall that this also enables a higher capacity compared to 50 vol %). In addition to a 0 s g^{-1} self-extinguishing time, EC/PC offers advantages in vapor flammability. Figure 1c and Supplementary Video 1 illustrate a vapor flammability test, in which 1 mL of EC/DEC and EC/PC with 20 vol % TEP additive was heated to 200 °C to generate significant vapor pressure. After a torch is held to both vials, the vapors from the EC/DEC/TEP electrolyte sustain a constant flame (Figure 1c, left vial), likely due to the high vapor pressure of DEC relative to EC and TEP. In contrast, the vapors of EC/PC/TEP are nonflammable (Figure 1c, right vial), likely because TEP boils at a lower temperature than EC/PC (solvent properties are listed in Table S1) and is known to suppress ignition even in the vapor phase.[22]

Next, we evaluate the impact of 20 vol % TEP on the battery performance by subjecting K||Gr cells to one formation cycle at C/20 and then 100 cycles at C/5 with upper and lower voltage cutoffs of 2 and 0 V, respectively. Specific discharge capacities for cells assembled with 1 M KPF_6 in EC/PC (black, hereon abbreviated to "EC/PC") and with 1 M KPF_6 in EC/PC with 20 vol % TEP (green, hereon abbreviated to "20% TEP") are shown in Figure 2a. In the C/20 formation step, 20% TEP outperforms EC/PC, with a higher initial Coulombic efficiency (ICE) of 79% compared to 72%. When the current increases to C/5 for the rest of cycling, 20% TEP can access a much higher capacity (260 mAh g^{-1} compared to 113 mAh g^{-1} for EC/PC). Over time, the capacity slowly fades in the 20% TEP electrolyte to 215 mAh g^{-1} by the 100th cycle at this rate (Figure S3). Note that EC/DEC + 20% TEP shows behavior similar to that of EC/PC + 20% TEP but is not intrinsically nonflammable (Figure S4).

To understand how the capacity fade in EC/PC + 20% TEP compares to other systems, we analyze the performance in high-loading K||HC cells (>3 mg cm^{-2}) over extended cycling

https://doi.org/10.1021/acsaem.4c02579
ACS Appl. Energy Mater. 2024, 7, 10245−10250

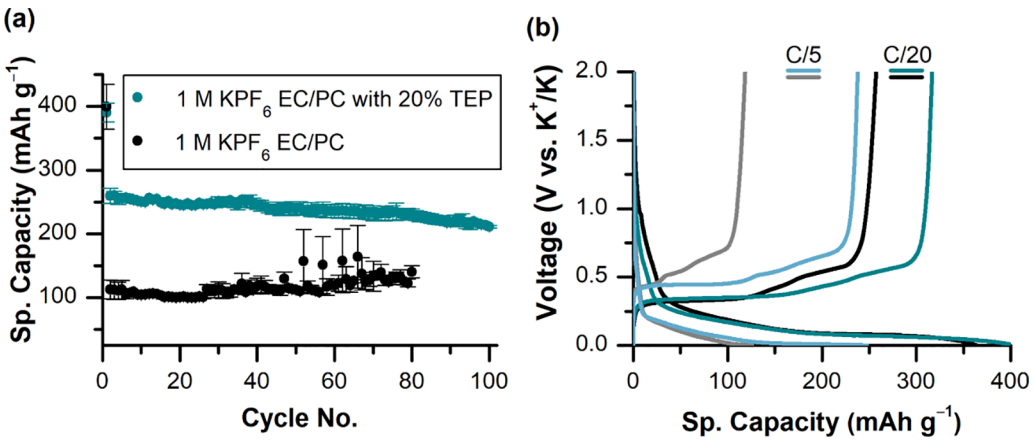

Figure 2. (a) Galvanostatic cycling of K||Gr half-cells with one formation step at *C*/20 and subsequent cycles at *C*/5 in 1 M KPF_6 in EC/PC with 20% TEP (green) and EC/PC (black). Individual points are the average of two cells, with the standard error represented via bars. The theoretical capacity for the formation of KC_8 is 279 mAh g^{-1}. (b) Voltage profiles of the formation and first *C*/5 cycle for K||Gr half cells cycled in EC/PC (formation in black; *C*/5 in gray) and EC/PC with 20% TEP (formation in green; *C*/5 in light blue).

and against another state-of-the-art KIB electrolyte, 3 M KFSI in EC/DEC,[23] in K||Gr cells. Figure S5 shows that, after 75 cycles, K||Gr cells cycled in EC/PC + 20% TEP and 3 M KFSI EC/DEC give equivalent CE values of 98.9% when cycled at *C*/5 and K||HC cells in EC/PC + 20% TEP to deliver CE = 99.6%. We suspect the lower CE of graphite may be due to differences in passivation and/or the volume changes that occur during potassiation/depotassion of graphite (K-ion intercalation into graphite results in 60% volume expansion[12]). In contrast, EC/PC cells maintain low capacity and exhibit capacity fluctuations that initially fade and then slowly increase with sporadic spikes. Eventually, cycling became so erratic that cells were removed from the cycler prior to 100 cycles (note that the first 80 cycles are shown for all cells in Figure 2).

We note that the compatibility of graphite with EC/PC + 20% TEP is unique to KPF_6. Figure S4 includes the capacity of Li||Gr cells assembled with the analogous $LiPF_6$ electrolyte. The capacity immediately decreased to ∼70 mAh g^{-1} and remained low for 100 cycles. Voltage profiles (Figure S6) and ^{17}O NMR spectra (Figure S7) indicate stronger coordination of Li^+ to PC, resulting in cointercalation and continuous SEI formation (discussed further in the Supporting Information).

The voltage profiles shown in Figure 2b aid in explaining how EC/PC + 20% TEP (green) enable higher capacity cycling in K||Gr cells. In the formation step, the shapes of the potassiation and depotassiation profiles look similar for both 20% TEP and EC/PC, although the higher ICE is clearly evident for EC/PC + 20% TEP. When the current increases to *C*/5, the cell overpotential increases and the onset potential of potassiation drops by 100 mV in both EC/PC and 20% TEP cells. However, the 20% TEP cells retain the potassiation voltage plateau, whereas the EC/PC profile is highly sloped and reaches a lower cutoff voltage and lower capacity. During depotassiation, the same 100 mV overpotential is observed, and the initial voltage plateau (now at 0.44 V) is only observed for the 20% TEP cells. This suggests that the final high-capacity phases of graphite potassiation (i.e., KC_8) form when cycling in 20% TEP but not when cycling in EC/PC. We confirmed this via ex situ XRD of potassiated graphite (Figure S8). After *C*/5 discharge to 0 V, the reflection at 33.3° for KC_8 formation is only observed in cells cycled in 20% TEP, in addition to reflections at 28.2° consistent with early-stage graphite-intercalated compounds.[24] As expected, graphite cycled in EC/PC shows a prominent reflection at 26.5° consistent with pristine graphite and no reflection for KC_8, indicative of incomplete potassiation.[24] Note that, although PC is known to intercalate with Li-ions, we do not believe that this is the case for EC/PC mixtures in KIBs. The intercalation voltage in Figure 1b remains low and is not consistent with solvent cointercalation; further, if the cycling rate is decreased to *C*/10, the overall capacity of EC/PC increases, ending at 178 mAh g^{-1} after 100 cycles (Figure S9), which is consistent with previous literature reports that show K-ion intercalation in Gr using EC/PC at slower rates.[5]

Graphite cycled in 20% TEP is clearly better able to retain capacity at higher current densities (∼56 mA g^{-1}). We assessed the bulk characteristics of cell components as the underlying cause; however, at room temperature, the ionic conductivity of 20% TEP slightly decreases to 8.0 mS cm^{-1} from 9.2 mS cm^{-1} measured for EC/PC (to retain high-rate capability, it is likely preferred to minimize TEP addition to the threshold composition for nonflammability). We note that the ionic conductivity of 20% TEP is still much higher than the 5.1 mS cm^{-1} recorded for 2 M KFSI TEP. Additionally, Raman spectroscopy shows that graphite electrodes cycled in either electrolyte have similar quantities of disordered phases generally attributed to capacity fade (Figure S10). These data suggest that the improvement in the rate capability lies in improved charge transfer at the graphite surface, potentially due to changes in the SEI composition after TEP addition.

To observe changes in the charge-transfer resistance from the SEI, we conducted potentiostatic electrochemical impedance spectroscopy (EIS). K||Gr cells underwent formation at *C*/20 and then potassiation to ∼50% state-of-charge (SOC) at 0.1 V and were held at a constant voltage for 2 h. The K||Gr cells were then disassembled and reassembled as symmetrical Gr||Gr cells to isolate the impedance spectra for graphite.[25,26] The results are shown in Figure 3. One dominant semicircle assigned to the charge-transfer impedance is observed and encompasses both diffusion through the SEI and K-ion solvation/desolvation.[27] When the collected EIS spectra are fitted to a simple Randles circuit (Figure 3, inset), R_{CT} is found to be 2467 Ω with 20% TEP and 3376 Ω with EC/PC (note: R_{CT} values from the fit are divided in half to find the single-electrode impedance; full fit parameters and errors are listed in Table S2).

https://doi.org/10.1021/acsaem.4c02579
ACS Appl. Energy Mater. 2024, 7, 10245−10250

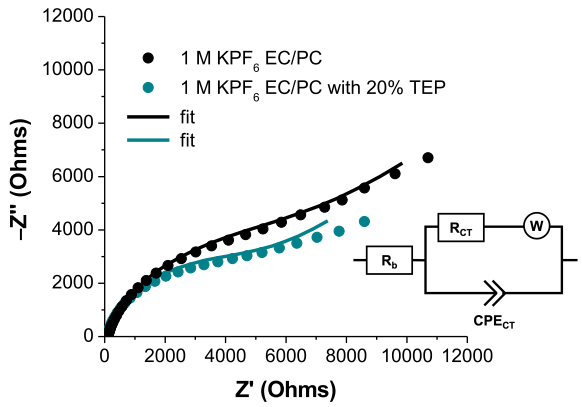

Figure 3. EIS of symmetric Gr||Gr cells after one *C*/20 formation step. Cells were cycled in 1 M KPF_6 with EC/PC (black) or EC/PC with 20 vol % TEP (green). Fits were generated using a Randles circuit (shown at the bottom right) and are plotted as solid lines.

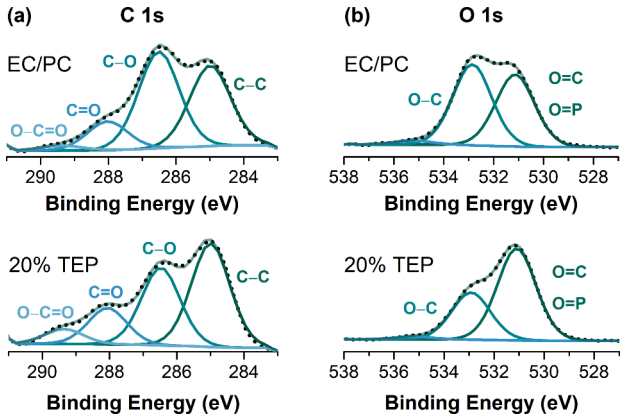

Figure 4. Ex situ XPS spectra of graphite anodes cycled opposite K metal for 20 cycles. (a) C 1s spectra of 1 M KPF_6 in EC/PC (top) and with 20% TEP (bottom). (b) O 1s spectra of 1 M KPF_6 in EC/PC (top) and with 20% TEP (bottom). Raw data are shown as black dots, and the summed peak envelope is shown as a transparent green line.

To determine how TEP alters the SEI, we characterized the surface layer formed on graphite electrodes after 20 cycles using air-free X-ray photoelectron spectroscopy (XPS). Figure 4a shows that cycling in the EC/PC electrolyte increases the proportion of C−O bonds (286.5 eV) observed in the C 1s orbital by 50% compared to cycling in 20% TEP (all XPS peak assignments and fractional abundances are listed in Table S3), indicating a much higher content of organic phases such as poly(ethylene oxide) and potassium alkoxide.[28] The accumulation of C−O species suggests increased SEI accumulation from carbonate reduction, consistent with the lower ICE observed during cycling and kinetic hindrance, leading to low capacity. The O 1s spectra in Figure 4b show that TEP addition results in a 40% increase in the proportion of highly oxygenated species (531.1 eV). The minority contribution of the O-C═O and C═O to the C 1s spectrum indicates that the O 1s peak at 531.1 eV is therefore likely made up of other phases, such as phosphates. P 2p spectra (Figure S11) for both electrolytes have two doublets, corresponding to residual KPF_6 and phosphate species. Distinguishing between fluorophosphates from KPF_6 breakdown (potentially present in both electrolytes) and phosphates produced from TEP reduction is not possible with XPS and necessitates other methods.

Higher chemical resolution of the phosphorus-containing SEI species is achieved via NMR spectroscopy. To generate a detectable quantity of electrolyte decomposition products for solution NMR, we constructed a K||Gr coin cell with high graphite mass loading (7 mg cm^{-2}). We conducted cyclic voltammetry on the cell at a very low scan rate (0.01 mV s^{-1}) between 0 and 1 V for 5 cycles. After disassembling the cell, we dissolved the graphite electrode in a 1:1 H_2O/D_2O mixture. Control experiments using an uncycled graphite electrode and pristine electrolyte yielded a ^{31}P NMR signal from solely TEP and KPF_6 (Figure S12). Therefore, we are confident that peaks in the ^{31}P NMR spectrum of the dissolved sample originate from the graphite interphase and not electrolyte hydrolysis.

In the ^{31}P NMR spectrum shown in Figure 5a, we observe two singlets near 0 ppm (full spectrum shown in Figure S13).

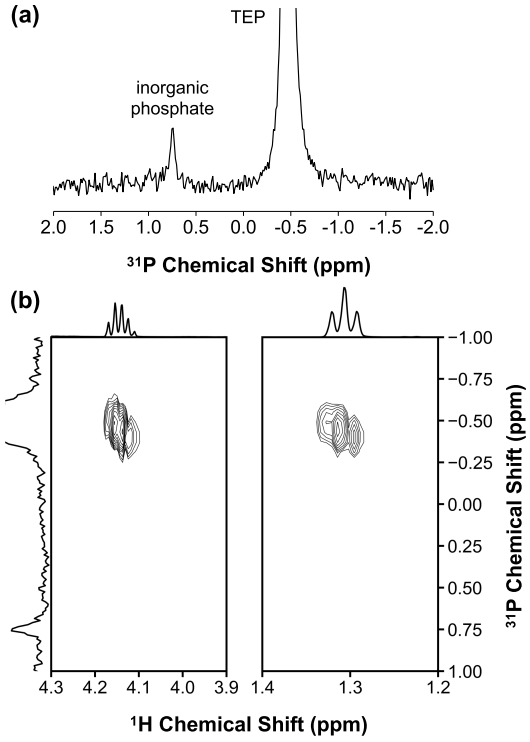

Figure 5. (a) 1D ^{31}P NMR and (b) 2D $^{1}H-^{31}P$ HMQC NMR of a graphite electrode cycled in 20% TEP from 0 to 1 V for 5 cycles and then dissolved in 1:1 D_2O/H_2O. The TEP peak is truncated to magnify the intensity of the phosphate decomposition product.

The largest singlet at −0.46 ppm is assigned to TEP. The other singlet appears slightly upfield of TEP at 0.77 ppm, consistent with increased shielding on the central P nucleus from the reductive decomposition of TEP to an inorganic potassium phosphate salt.[29] (Note that this peak at 0.77 ppm is not observed when a half-cell is cycled in the control EC/PC electrolyte (Figure S14) and is observed when a half-cell is cycled in 1 M KFSI in EC/PC with 20% TEP (Figure S15), supporting that it is a byproduct of TEP and not the hexafluorophosphate anion.) To confirm whether the TEP reduction product is an organophosphate or a free phosphate anion, we conducted 2D $^{31}P\{^{1}H\}$ heteronuclear multiple quantum correlation (HMQC) NMR (Figure 5b). In this experiment, the peaks that appear represent ^{31}P nuclei coupled to nearby ^{1}H nuclei. For example, the ^{31}P singlet for TEP at −0.46 ppm yields 2D-correlated cross-peak intensities at 4.1

https://doi.org/10.1021/acsaem.4c02579
ACS Appl. Energy Mater. 2024, 7, 10245−10250

ppm (dq, J_{H-P} = 1 Hz) and 1.3 ppm (dt, J_{H-P} = 0.9 Hz) in the ^{1}H NMR spectrum, representing the ethyl and methyl protons in the alkyl chains, respectively. There is no observed signal intensity for the ^{31}P singlet at 0.77 ppm, suggesting no nearby ^{1}H from the alkyl chains. Therefore, we assign the shift to inorganic potassium phosphates in the graphite SEI.

Improvements in capacity retention and charge transfer are often correlated to increased quantities of inorganic phases in the SEI, such as metal fluorides.[1,7] However, previous work from our group indicates that KPF_6 is stable at low potentials, mitigating anionic decomposition.[13] Indeed, solution-state ^{19}F NMR of the dissolved graphite electrodes exhibit no peaks at lower frequencies assigned to F^- (e.g., −125 ppm) from dissolved KF (Figure S16). Analysis of the F 1s orbital in XPS indicates that both electrolytes yield KF in the SEI (Figure S17), suggesting that there is a discrepancy between these two analytical techniques. In Li-based systems, beam damage in XPS has been repeatedly shown to artificially increase the LiF content from Li salt exposure to X-rays,[30] and we believe that the same phenomenon may be occurring in our experiments. Therefore, we cannot reliably attribute the improved capacity retention and reduced R_{CT} to an increasingly fluorinated SEI, as is often suggested in the literature—or at the very least, this suggests that there are alternative methods to achieving these performance outcomes. We posit that the products of phosphate reduction improve surface passivation over carbonate-derived SEI components. This is an exciting outcome because it is the first demonstration that one can utilize low-concentration phosphorus-containing electrolyte solvents to incorporate ionically conductive components into the SEI of KIB anodes to improve performance at appreciable rates for carbonate-based systems. We also note that, due to the stability of K salts in the 1 M concentration regime, this approach may provide a route to eliminate fluorine in the battery altogether, mitigating the generation of hazardous byproducts produced during electrochemical cycling.

In summary, we find that 1 M KPF_6 in EC/PC with 20% TEP serves as a compelling electrolyte that opens up the design space for low-concentration KIB electrolytes that may offer a wellspring of properties, including fire resistance and low toxicity. The combination of cyclic carbonates and phosphates, specifically, offers intrinsic nonflammability in both liquid and vapor phases, relatively high ionic conductivity compared to HCEs with TEP as the sole solvent, and compatibility with K-ion intercalation into graphite at low salt concentration. EC, PC, and TEP are all affordable and mass-produced. Moreover, the TEP cosolvent appears to reduce the overpotential and improve the capacity retention of graphite. The inorganic phosphate salts produced in the interphase, here characterized for the first time by NMR techniques, likely aid in passivation of the surface and prevent carbonate reduction to soluble organic species. Prior to this report, low-concentration TEP-based electrolytes have exhibited poorly passivating SEIs that lead to KIB performance degradation (e.g., Figure S2 shows that 1 M KPF_6 in TEP results in frequent shorts when used in half-cell testing and almost no reversible capacity while 1 M KFSI in TEP has been shown to lose ∼40% capacity in 25 cycles[6]). This work clearly provides a platform where one can construct a safe, low-concentration electrolyte that is compatible with graphite in KIBs and through the use of routine optimization strategies (e.g., additives and formation protocols) maximize performance. Additionally, future work remains to optimize electrolytes for the higher graphite loadings expected in commercial cell formats, as well as cathode materials and coatings that are compatible with these more conventional electrolyte formulations.

Interestingly, combinations of cyclic carbonates and organophosphates were explored for flame-retardant LIB electrolytes over 20 years ago[21] but were abandoned due to very poor cycling performance from cointercalation and continuous solvent decomposition. In addition, we know from decades of research on LIBs that $LiPF_6$ readily reduces at the anode to form LiF that is embedded in the SEI. When using NMR spectroscopy, which does not reduce the KPF_6 salt, we see no evidence of KF in the SEI for either electrolyte formulation. With the present results in hand, we stress that the electrolyte and electrode surface design space beyond Li-ion systems may be counterintuitive and much more expansive than we originally thought. We must continue to reassess design principles to take advantage of the unique properties and opportunities presented by alternative battery chemistries.

■ ASSOCIATED CONTENT

Supporting Information

The Supporting Information is available free of charge at https://pubs.acs.org/doi/10.1021/acsaem.4c02579.

Experimental methods, additional electrochemistry, XRD, Raman spectroscopy, additional XPS, additional solution NMR, list of solvent properties, and EIS fit parameters (PDF)

Footage of vapor flammability test of EC/DEC/TEP and EC/PC/TEP solutions (Supplementary Video 1) (MP4)

■ AUTHOR INFORMATION

Corresponding Author

Lauren E. Marbella − *Department of Chemical Engineering, Columbia University, New York, New York 10027, United States;* orcid.org/0000-0003-1639-3913; Email: lem2221@columbia.edu

Authors

Andrew W. Ells − *Department of Chemical Engineering, Columbia University, New York, New York 10027, United States;* orcid.org/0000-0002-5015-3991

Pablo J. Buitrago Botero − *Department of Chemical Engineering, Columbia University, New York, New York 10027, United States;* orcid.org/0009-0009-6131-8657

Bret Schumacher − *Department of Earth and Environmental Engineering, Columbia University, New York, New York 10027, United States;* orcid.org/0000-0002-5186-5325

Lakshmi Bhai − *Department of Chemical Engineering, Columbia University, New York, New York 10027, United States; Department of Chemistry, Columbia University, New York, New York 10027, United States;* orcid.org/0009-0001-0581-5247

Complete contact information is available at: https://pubs.acs.org/10.1021/acsaem.4c02579

Notes

The authors declare no competing financial interest.

https://doi.org/10.1021/acsaem.4c02579
ACS Appl. Energy Mater. 2024, 7, 10245−10250

■ ACKNOWLEDGMENTS

This work was supported by the National Science Foundation (DMR-2116728). A.W.E. is supported by the U.S. Department of Defense through the National Defense Science & Engineering Graduate Fellowship program. L.E.M. is supported by the Provost's Postdoctoral Research Scientist and Scholar Program. Research reported in this publication was supported by the Office of The Director of the National Institutes of Health under Award S10OD026749. The content is solely the responsibility of the authors and does not necessarily represent the official views of the National Institutes of Health. We thank Prof. Dan Steingart for access to laboratory supplies and space for safety testing. We thank Dr. Jon Decatur for aid in designing 2D NMR experiments. We thank Dr. Tai-De Li for assistance in collecting the XPS data at the City University of New York Advanced Science Research Center. We thank Dr. Philippe Chow for assistance in setting up the Raman spectroscopy experiments.

■ REFERENCES

(1) Hosaka, T.; Kubota, K.; Hameed, A. S.; Komaba, S. Research Development on K-Ion Batteries. *Chem. Rev.* **2020**, *120*, 6358−6466.

(2) Dhir, S.; Wheeler, S.; Capone, I.; Pasta, M. Outlook on K-Ion Batteries. *Chem.* **2020**, *6* (10), 2442−2460.

(3) Vaalma, C.; Buchholz, D.; Weil, M.; Passerini, S. A Cost and Resource Analysis of Sodium-Ion Batteries. *Nat. Rev. Mater.* **2018**, *3* (18013), 1−11.

(4) Komaba, S.; Hasegawa, T.; Dahbi, M.; Kubota, K. Potassium Intercalation into Graphite to Realize High-Voltage/High-Power Potassium-Ion Batteries and Potassium-Ion Capacitors. *Electrochem. Commun.* **2015**, *60*, 172−175.

(5) Zhao, J.; Zou, X.; Zhu, Y.; Xu, Y.; Wang, C. Electrochemical Intercalation of Potassium into Graphite. *Adv. Funct Mater.* **2016**, *26* (44), 8103−8110.

(6) Liu, S.; Mao, J.; Zhang, Q.; Wang, Z.; Pang, W. K.; Zhang, L.; Du, A.; Sencadas, V.; Zhang, W.; Guo, Z. An Intrinsically Non flammable Electrolyte for High Performance Potassium Batteries. *Angew. Chem. Int. Ed* **2020**, *59*, 3638−3644.

(7) Zeng, G.; Xiong, S.; Qian, Y.; Ci, L.; Feng, J. Non-Flammable Phosphate Electrolyte with High Salt-to-Solvent Ratios for Safe Potassium-Ion Battery. *J. Electrochem. Soc.* **2019**, *166* (6), A1217−A1222.

(8) WU, X.; Qiu, S.; Liu, Y.; Xu, Y.; Jian, Z.; Yang, J.; Ji, X.; Liu, J. The Quest for Stable Potassium Ion Battery Chemistry. *Adv. Mater.* **2022**, *34*, 2106876.

(9) Deng, L.; Qu, J.; Niu, X.; Liu, J.; Zhang, J.; Hong, Y.; Feng, M.; Wang, J.; Hu, M.; Zeng, L.; Zhang, Q.; Guo, L.; Zhu, Y. Defect-Free Potassium Manganese Hexacyanoferrate Cathode Material for High-Performance Potassium-Ion Batteries. *Nat. Commun.* **2021**, *12* (1), 1−9.

(10) Hess, S.; Wohlfahrt-Mehrens, M.; Wachtler, M. Flammability of Li-Ion Battery Electrolytes: Flash Point and Self-Extinguishing Time Measurements. *J. Electrochem. Soc.* **2015**, *162* (2), A3084−A3097.

(11) Ponrouch, A.; Marchante, E.; Courty, M.; Tarascon, J. M.; Palacín, M. R. In Search of an Optimized Electrolyte for Na-Ion Batteries. *Energy Environ. Sci.* **2012**, *5* (9), 8572−8583.

(12) Jian, Z.; Luo, W.; Ji, X. Carbon Electrodes for K-Ion Batteries. *J. Am. Chem. Soc.* **2015**, *137* (36), 11566−11569.

(13) Ells, A. W.; May, R.; Marbella, L. E. Potassium Fluoride and Carbonate Lead to Cell Failure in Potassium-Ion Batteries. *ACS Appl. Mater. Interfaces* **2021**, *13* (45), 53841−53849.

(14) Bie, X.; Kubota, K.; Hosaka, T.; Chihara, K.; Komaba, S. A Novel K-Ion Battery: Hexacyanoferrate(ii)/Graphite Cell. *J. Mater. Chem. A Mater.* **2017**, *5* (9), 4325−4330.

(15) Stoebe, T. G. Influence of OH- Ions on Infrared Absorption and Ionic Conductivity in Lithium Fluoride Crystals. *J. Phys. Chem. Solids* **1967**, *28*, 1375−1382.

(16) Lowndes, R.; Martin, D. Dielectric Constants of Ionic Crystals and Their Variations With Temperature and Pressure. *Proc. R. Soc. London A* **1970**, *316* (1526), 351−375.

(17) Yildirim, H.; Kinaci, A.; Chan, M. K. Y.; Greeley, J. P. First-Principles Analysis of Defect Thermodynamics and Ion Transport in Inorganic SEI Compounds: LiF and NaF. *ACS Appl. Mater. Interfaces* **2015**, *7* (34), 18985−18996.

(18) Terborg, L.; Nowak, S.; Passerini, S.; Winter, M.; Karst, U.; Haddad, P. R.; Nesterenko, P. N. Ion Chromatographic Determination of Hydrolysis Products of Hexafluorophosphate Salts in Aqueous Solution. *Anal. Chim. Acta* **2012**, *714*, 121−126.

(19) Deng, L.; Zhang, Y.; Wang, R.; Feng, M.; Niu, X.; Tan, L.; Zhu, Y. Influence of KPF6 and KFSI on the Performance of Anode Materials for Potassium-Ion Batteries: A Case Study of MoS2. *ACS Appl. Mater. Interfaces* **2019**, *11* (25), 22449−22456.

(20) Mosin, D. N.; Marks, E. A.; Burmakin, E. I.; Molchanova, N. G.; Shekhtman, G. Sh. Electroconduction of Potassium, Rubidium, and Cesium Orthophosphates. *Russ. J. Electrochem* **2001**, *37* (8), 863−864.

(21) Wang, X.; Yasukawa, E.; Kasuya, S. Nonflammable Trimethyl Phosphate Solvent-Containing Electrolytes for Lithium-Ion Batteries: I. Fundamental Properties. *J. Electrochem. Soc.* **2001**, *148* (10), A1058.

(22) Wang, J.; Yamada, Y.; Sodeyama, K.; Watanabe, E.; Takada, K.; Tateyama, Y.; Yamada, A. Fire-Extinguishing Organic Electrolytes for Safe Batteries. *Nat. Energy* **2018**, *3* (1), 22−29.

(23) Igarashi, D.; Kubota, K.; Hosaka, T.; Tatara, R.; Inose, T.; Ito, Y.; Inoue, H.; Takeuchi, M.; Komaba, S. Effect of Crystallinity of Synthetic Graphite on Electrochemical Potassium Intercalation into Graphite. *Electrochemistry* **2021**, *89* (5), 433−438.

(24) Onuma, H.; Kubota, K.; Muratsubaki, S.; Ota, W.; Shishkin, M.; Sato, H.; Yamashita, K.; Yasuno, S.; Komaba, S. Phase Evolution of Electrochemically Potassium Intercalated Graphite. *J. Mater. Chem. A* **2021**, *9*, 11187−11200.

(25) Hosaka, T.; Muratsubaki, S.; Kubota, K.; Onuma, H.; Komaba, S. Potassium Metal as Reliable Reference Electrodes of Nonaqueous Potassium Cells. *J. Phys. Chem. Lett.* **2019**, *10* (12), 3296−3300.

(26) Liu, P.; Mitlin, D. Emerging Potassium Metal Anodes: Perspectives on Control of the Electrochemical Interfaces. *Acc. Chem. Res.* **2020**, *53* (6), 1161−1175.

(27) Xu, K.; Von Cresce, A.; Lee, U. Differentiating Contributions to "Ion Transfer" Barrier from Interphasial Resistance and Li^+ Desolvation at Electrolyte/Graphite Interface. *Langmuir* **2010**, *26* (13), 11538−11543.

(28) Caracciolo, L.; Madec, L.; Martinez, H. XPS Analysis of K-Based Reference Compounds to Allow Reliable Studies of Solid Electrolyte Interphase in K-Ion Batteries. *ACS Appl. Energy Mater.* **2021**, *4* (10), 11693−11699.

(29) Maier, L.; Van Wazer, J. R. Principles of Phosphorus Chemistry. *J. Am. Chem. Soc.* **1962**, *84* (16), 3054−3058.

(30) Yu, W.; Yu, Z.; Cui, Y.; Bao, Z. Degradation and Speciation of Li Salts during XPS Analysis for Battery Research. *ACS Energy Lett.* **2022**, *7* (10), 3270−3275.

https://doi.org/10.1021/acsaem.4c02579
ACS Appl. Energy Mater. 2024, 7, 10245−10250